Numerical Analysis and Experimental Validation of a Submerged Inlet on the Plane Surface

SUN Shu, GUO Rong-wei
(Internal Flow Research Center, Nanjing University of Aeronautics and Astronautics, Nanjing 210016, China)

Abstract: In order to get a deep insight of a submerged inlet on the plane surface, the integrated flow field of the inlet and fuselage has been numerically studied. The investigation is mainly focused on the formation of the total pressure distribution at the exit of the inlet, the structure of the inner flow and the effects of the boundary layer along the fuselage on the performance of the inlet. Moreover, in comparison with the experimental data at different angles of attack, yaws and mass flow ratios, the reliabilities of the computational fluid dynamics(CFD) studied are verified. Results indicate: (1) the CFD results agree well with the experiment results and the relative errors of the total pressure coefficient is less than 1%; (2) at the inlet's exit, the contour of total pressure obtained by CFD is similar to the experiment result except the contour in the low total pressure zone in CFD is slightly larger; (3) the secondary flow at the cross section behave as two counter-rotating vortices. Along the flow direction, the fields influenced by the vortex pair transport downstream and expand to the whole section at the exit; (4) the total pressure loss at the exit of the submerged inlet can be divided into external loss and internal loss. Usually, the external loss is greater than the internal loss, and both decrease with the augment of the Mach number at the exit. In addition, when the angle of attack ranges from -2° to 8°, the total pressure coefficient ascends gradually, due to the reduction of the external loss caused by the less boundary layer flow captured and the invisible change of the internal loss.

Key words: submerged inlet on the plane surface; CFD; boundary layer; counter-rotating vortices; total pressure coefficient

平面埋入式进气道的数值仿真研究与试验验证. 孙姝, 郭荣伟. 中国航空学报(英文版), 2005, 18(3): 199-205.

摘 要: 通过对比平面埋入式进气道的流量特性、攻角特性和侧滑角特性的计算和试验结果, 验证了本文数值方法的可靠性。在此基础上, 利用 CFD 技术分析了其出口总压图谱的成因, 探讨了该类进气道的内流场结构并分析了弹身附面层的影响。研究结果表明: (1) 本文所采用的数值分析方法具有较高的精度, 所预测的进气道出口截面总压恢复系数的相对误差在 1% 以内; (2) 计算所得到的进气道出口截面高压区位置以及范围大小与试验结果相当吻合, 但低压区范围稍大; (3) 平面埋入式进气道沿程截面二次流的速度较大, 表现为一对反向对涡。随着沿程截面的由前而后, 该对涡的影响区域不断扩大, 直至整个内通道中; (4) 埋入式进气道出口截面的总压损失可分为管道外部损失和管道内部损失两部分。研究范围内进气道的外部总压损失要大于内部总压损失, 且随着进气道平均出口马赫数的增高, 外部总压损失和内部总压损失均逐渐降低。此外, 当攻角从 -2° 变化到 8° 时, 由于进入进气道内的附面层气流减少, 管道外部总压损失不断下降, 而其内部总压恢复系数的变化趋势并不明显, 因而总压恢复系数随着攻角的增加而增加。

关键词: 平面埋入式进气道; CFD; 弹身附面层; 流量特性; 攻角特性; 侧滑角藤性; 二次流; 反向对涡; 总压恢复系数

文章编号: 1000-9361(2005)03-0199-07 中图分类号: V211.3 文献标识码: A

Having advantageous geometrical characteristics, a submerged (also known as flush mounted)

Received date: 2004-08-17; Revision received date: 2004-12-29
Foundation item: National 973 Plan of China

inlet has received considerable attention. This type of inlet is superior to fuselage-nose or wing-leading-edge inlet in the following respects: (1) short internal ducting bends with a saving in weight, (2) less external drag, (3) minimization of foreign object damage, (4) low observability characteristics. Thus, in the early forties of the 20th century, research studies were initiated for the so called NACA submerged inlet. This preliminary study was pursued by detailed investigations mainly on the design and experiment of the inlet[1-9]. However, the revealment for the complex phenomena of the submerged inlet is restricted with the current conditions of wind-tunnel experiments and measurements.

Recently, with the development of the computer technology, the Computational Fluid Dynamics(CFD) is employed for the submerged inlet. Some numerical analyses and a design optimization study are conducted on the submerged inlet with round fuselage[10-12]. But little work was done on the internal flow structure and air-admission mechanism, and let alone the wind-tunnel experimental validation of CFD results at high subsonic.

In order to get a deep insight of a submerged inlet on the plane surface, the integrated flow field of the inlet and fuselage is numerically studied. The investigation is mainly focused on the formation of the total pressure distribution at the exit of the inlet, the structure of the inner flow and the effects of the boundary layer along the fuselage on the performance of the inlet. Moreover, in comparison with the experimental data at different angles of attack, yaws and mass flow ratios, the reliabilities of the CFD studied are verified.

1 Numerical Approach

1.1 Inlet and fuselage

A drawing of the fuselage and the submerged inlet can be seen in Fig. 1. The inlet is placed at the aft part of the fuselage which is of trapezoid cross section. The distance from the apex of the fuselage to the fore lip of the diffuser is $12D$, where D is the diameter of the inlet's exit. As shown in Fig. 1, the total length of the inlet is $4.5D$ and the offset is $0.87D$ which is the distance between the central point of the exit and the abdomen plane of the fuselage. In addition, a trapezoid-like entrance of the inlet with side edge angle of 7.5°[13] is adopted in the sduty.

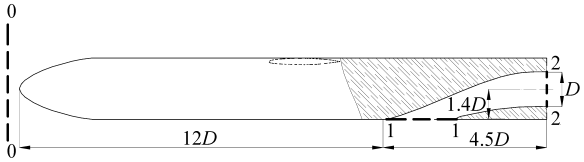

Fig. 1 Sketch of the inlet

1.2 Flow domain and boundary

The flow domain is split into two parts, namely, the fuselage zone and the channel zone. In order to eliminate the effects of boundary condition on the CFD results, a large column flow domain, with $20D$ in diameter and $30D$ in length, is chosen and the channel zone is extruded $2D$ at the actual exit of the inlet. Furthermore, the fuselage zone is solved using free stream condition at the entrance plane, a no-slip adiabatic boundary condition at the solid wall and subsonic outflow conditions with specified back pressure equal to the free stream value at the exit plane. In the computational process the solution obtained from the fuselage zone is used as an inflow boundary condition for the channel zone for which a back pressure is specified at the exit of the diffuser.

1.3 Grid generation

The grid topology used for the computations contains 21 blocks, which match completely each other and compose the complex flow domain, and the total number of grid points is approximately 900 000. A close up view of the surface grids around the entrance of the inlet is shown in Fig. 2(a) and also a side view of grids on the symmetry plane is presented in Fig. 2(b). It is found that clustering near the wall region and the channel zone is done by specifying the first cell height and the stretching ratio.

1.4 Flow solver

Utilizing a finite volume spatial discretization in which the state variables are stored at the cell center, the flow solver solves the Reynolds-averag

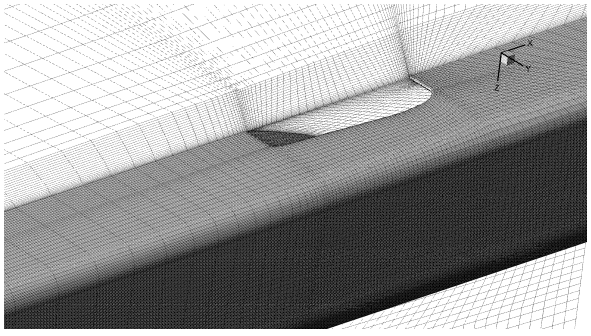

(a) Surface grids around the entrance of the inlet

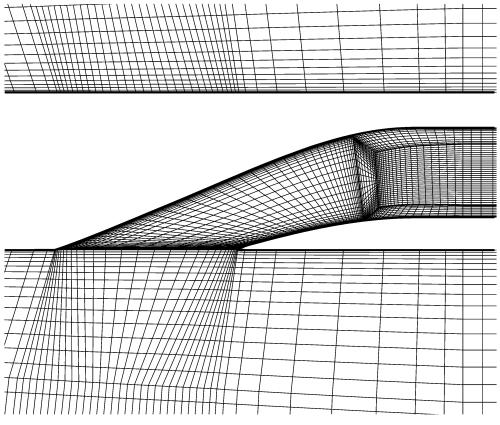

(b) Grids of the symmetry plane

Fig. 2 Grids of the submerged inlet on the plane surface

ed compressible time dependent Navier Stokes equations in three dimensions. In the computations, the inviscid flux scheme is Roe's Method and MUSCL approach is used for variable extrapolation. Turbulence is modeled by the $k-\varepsilon$ equations. A steady state solution is obtained by the Gauss Seidel relaxation scheme.

2 Numerical Analysis and Experimental Validation

In order to get a good knowledge of the flow characteristics of the submerged inlet on the plane surface, the numerical study is performed, of which the results are validated by the experimental data at different angles of attack, yaw and mass flow ratio.

2.1 Total pressure recovery coefficient at different Mach number at the exit

Unlike pitot inlet or S shaped inlet[14,15], the capture area of the submerged inlet is difficult to be determined. Therefore, the Mach number at the exit is used instead of the mass flow ratio in the analysis. Fig. 3 presents the total pressure recovery coefficient σ versus the Mach number at the exit. It can be noted that the CFD and experimental values match reasonably well, except at the high Mach number where the relative errors reach 1%. Additionally, the trend of the total pressure recovery with the exit Mach number is explained by Fig. 4, in which at the lower mass flow ratio ($Ma=0.33$) more low energy flow near the fuselage enters the inlet relative to the total mass flow captured.

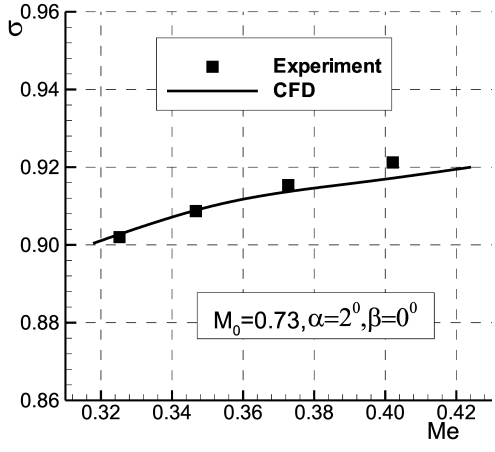

Fig. 3 Total pressure recovery coefficient versus Mach number at the exit

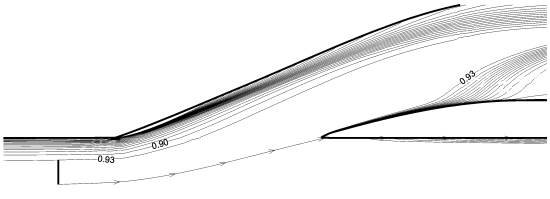

(a) Mach number 0.42 at the exit

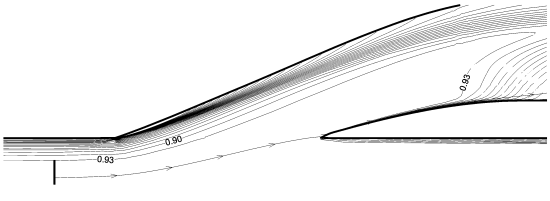

(b) Mach number 0.33 at the exit

Fig. 4 Entering high energy flow at different Mach number at the exit

2.2 Total pressure recovery coefficient at different angles of attack

Fig. 5 demonstrates the variation of total pres-

sure recovery coefficient σ with angles of attack α that range from − 2° to 8°. As shown in Fig. 5, the CFD result agrees well with the experimental data and the maximum difference is less than 0.01. Moreover, it can be observed that with the ascent of the incidence σ goes up and reaches over 0.95 at α= 8°. This tendency is interpreted as follows: on the one hand, with the angle of attack rising, the entrance of the submerged inlet is exposed to free stream more and more, resulting in more main flow captured and thereby the increase of total pressure recovery coefficient. On the other hand, in the case of high incidence, the counter-rotating vortex pair developed by the upwash flow around the fuselage sweeps away part of the boundary flow in front of the inlet which is pictured in Fig. 6, also causing the augment of σ.

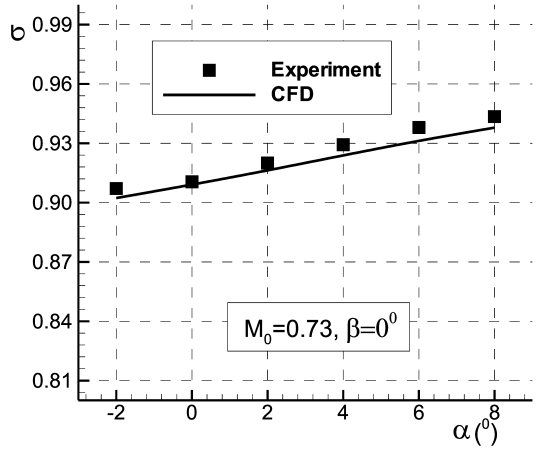

Fig. 5 Total pressure recovery coefficient versus angle of attack

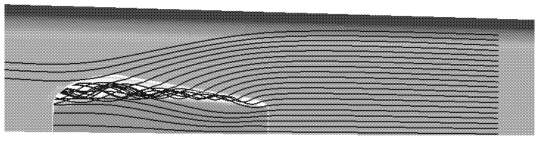

(a) Streamlines at α= 0°

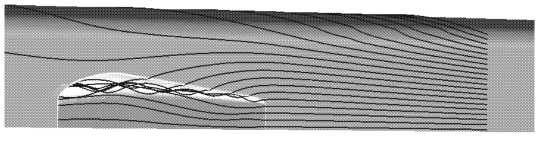

(b) Streamlines at α= 8°

Fig. 6 Streamlines released from the fuselage at different angles of attack

2.3 Effects of yaw on the total pressure recovery coefficient

The effects of yaw β on total pressure recovery coefficient σ are displayed in Fig. 7. When yaw is increased to 2°, the total pressure recovery coeffocoent σ achieves the highest value. It may be due to the reduction of the developing length of the boundary layer along the surface of the fuselage at yaw. As the yaw continues to move up to 6°, σ decreases to less than 0.91 because flow separation occurs at the lee side of the diffuser.

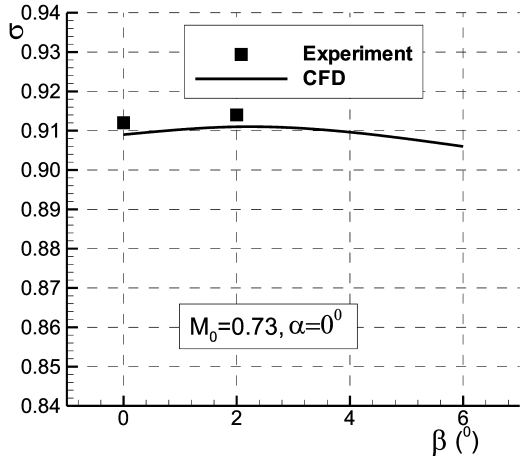

Fig. 7 Total pressure recovery versus yaw

2.4 Total pressure contours

Fig. 8 illustrates the total pressure recovery coefficient distribution at the exit of the inlet. Comparing the experiment with the computation, reasonable agreement can be seen in the high total pressure region at the upper part of the plot. Also, the maximum total pressure value and the total pressure range in the two contours are in very good agreement. Whereas, the size of the low total pressure region is a little larger in computation, which is subject to further investigation. The reason for the formation of low total pressure region at the exit is evident from the streamlines (Fig. 9). The boundary flow which is driven by the transverse pressure gradient and the secondary flow, thickening along the channel, is swept to the bottom of the diffuser yielding the low total pressure region at the exit.

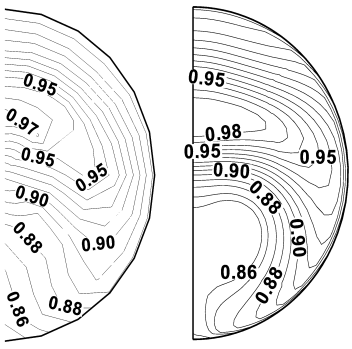

Experimental results CFD results

Fig. 8 Contours of total pressure recovery at the exit of the inlet

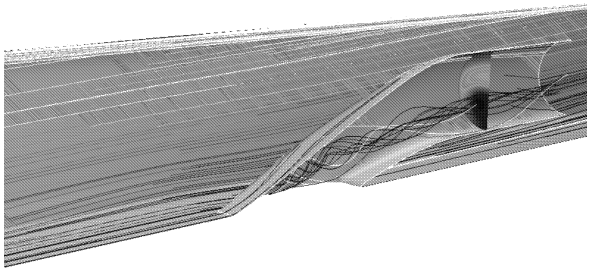

Fig. 9 Formation of the total pressure distributions at the exit of the inlet

2.5 Stucture of internal flow

The static pressure coefficient distribution and the velocity vector around the entrance on the symmetry plane are exhibited in Fig. 10. It can be inferred that the pressure gradient perpendicular to the freestream caused by the low static pressure at the fore lip forces the coming flow to enter the inlet.

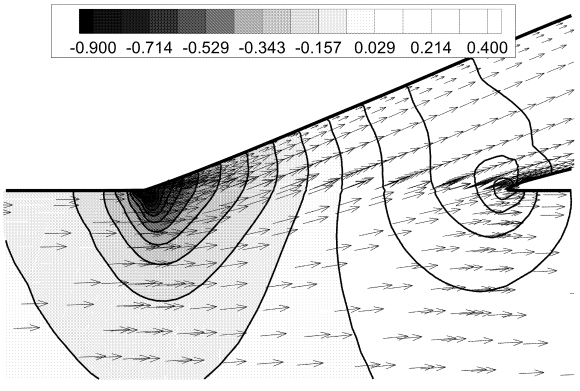

Fig. 10 Distributions of the static pressure coefficient and the velocity vector at the entrance of the inlet

A clear picture of the internal flow is shown in Fig. 11, where the development of secondary flow vectors along the duct is displayed. At the entrance, a counter-rotating vortex pair[15, 16] originated from side edge angle of 7.5° induces a downward velocity component which draws more and more main flow into the diffuser along the flow direction. As the flow goes downstream into the duct, another counter-rotating vortex pair due to the duct curvature strengthens the swirl motion created before, expands the fields of the secondary flow to the whole section at the exit. Consequently, the strong vortex pair occupies the bottom of the exit which is the deficit of the total pressure recovery(Fig. 8).

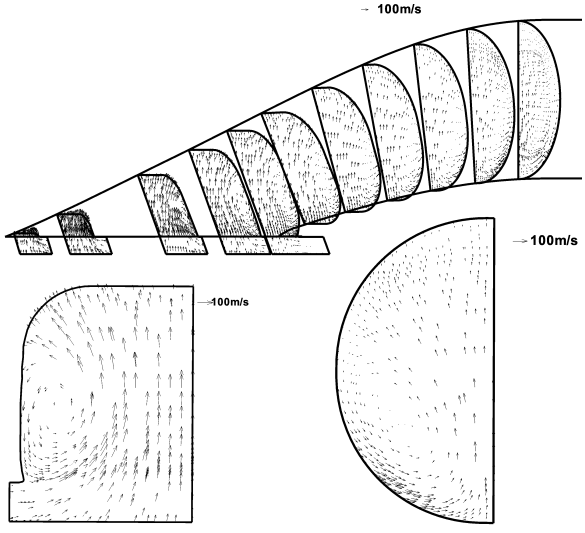

Fig. 11 Development of the secondary flow in the duct

In general, the pressure gradient perpendicular to the freestream at the fore lip and the counter-rotating vortex pair are the main impetus that inhale the main flow into the submerged inlet.

2.6 Effects of the boundary layer along the fuselage

For a deep study of the effects of the boundary layer along the fuselage on the aerodynamic performance of the submerged inlet on the plane surface, the total pressure recovery coefficient at the exit can be divided into the external total pressure recovery coefficient σ_1 which reflects the loss from the boundary layer of the fuselage, and the internal total pressure recovery coefficient σ_2 which repre-

sents the loss inside the duct. In the study, σ_1 and σ_2 are defined as follows

$$\sigma_1 = P_1^* / P_0^* \quad (1)$$

$$\sigma_2 = P_2^* / P_1^* \quad (2)$$

where, P_0^* is the total pressure of freestream marked 0-0 in Fig. 1; P_1^* is the total pressure of the flow at the entrance, and P_2^* is the total pressure at the exit. It is obvious that the total pressure recovery coefficient of the inlet is the product of σ_1 and σ_2.

Fig. 12 presents the total pressure recovery coefficients σ_1, σ_2 and σ as a function of the Mach number at the exit. It is not difficult to find that σ_1 is lower than σ_2, in that words, the total pressure loss as a result of boundary layer along the fuselage is greater than that from the flow mixing, the adverse pressure gradient and the friction in the duct. Also, it can be noted that with the enhancement of the Mach number at the exit, σ_1 and σ_2 both rise. For the case of σ_1, when the Me increases, less boundary flow relative to the total mass flow capture enters the inlet (referring to Fig. 4) which leads to the decline in the external total pressure loss. For the case of σ_2, despite the greater friction loss of the internal flow, a higher Me reduces the loss created by the adverse pressure gradient, so that when M_2 varies from 0.318 to 0.424 and M_1 correspondingly changes from 0.727 to 0.690 the internal total pressure loss decreases.

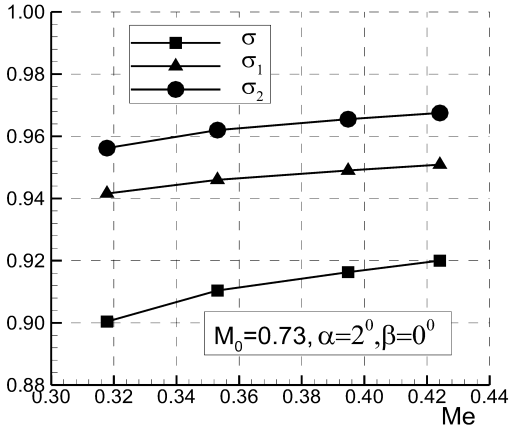

Fig. 12 σ_1, σ_2 and σ versus Mach number at the exit

Fig. 13, in which σ_1 increases and σ_2 keeps

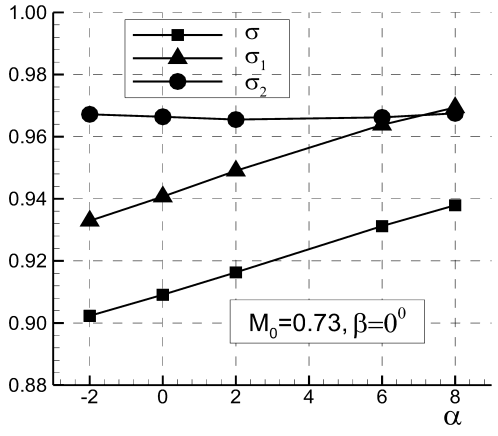

Fig. 13 σ_1, σ_2 and σ versus angle of attack

stable, suggests that with the angle of attack varying from $-2°$ to $8°$ the boundary layer along the fuselage plays a leading role in the total pressure loss of the inlet. The interpretation can be given from two aspects. When the incidence goes up, less boundary layer developed by the fuselage is involved into the duct shown in Fig. 6, resulting in the drop of the external total pressure loss. Furthermore, at the same M_2, with the variation of the incidence M_1 maintains the value of 0.72 or so, which implies that no obvious change is brought to the structure of internal flow and adverse pressure gradient of the duct, hence the internal total pressure loss remains almost constant.

In a word, the boundary layer along the fuselage possess a high portion of the total loss of the inlet and attaches great importance to the aerodynamic performance of the submerged inlet on the plane surface.

3 Conclusions

By numerical analysis and experimental validation of the submerged inlet on the plane surface, some conclusions can be reached as follows:

(1) The CFD results agree well with the experimental results and the relative errors of the total pressure recovery coefficient is less than 1%.

(2) At the inlet's exit, the contour of total pressure recovery obtained by CFD is similar to that obtained by the experiment except the low total pressure zone in CFD is slightly larger.

(3) The secondary flow at the cross sections behaves as two counter-rotating vortices. Along the flow direction, the fields influenced by the vortex pair transport downstream and expand to the whole section at the exit.

(4) The total pressure loss at the exit of the submerged inlet can be divided into external loss and internal loss. Usually, the external loss is greater than the internal loss, and both decrease with the augment of the Mach number at the exit. In addition, when the angle of attack ranges from -2° to 8°, the total pressure recovery coefficient ascends gradually, due to the reduction of the external loss caused by less boundary layer flow captured and the invisible change of the internal loss.

References

[1] Seddon J, Goldsmith E L. Intake aerodynamics[M]. London: Blackwell Science, 1999.

[2] 翁培奋. 埋入式进气道内外流场的数值计算和实验研究[D]. 南京航空航天大学, 1986.
Weng P F. Two-dimensional numerical and experimental investigation of a submerged inlet[D]. Nanjing University of Aeronautics and Astronautics, 1986. (in Chinese)

[3] 杨爱玲, 郭荣伟. 二维埋入式进气道的数值分析[J]. 航空学报, 1999, 20(5): 450-454.
Yang A L, Guo R W. Numerical simulation of the flow of two-dimensional submerged air inlet[J]. Acta Aeronautica et Astronautica Sinica, 1999, 20(5): 450-454. (in Chinese)

[4] 杨爱玲, 郭荣伟. 埋入式进气道设计及其气动性能研究[J]. 空气动力学报, 1998, 16(2): 154-161.
Yang A L, Guo R W. An investigation on design and performance for a submerged air inlet[J]. Acta Aerodynamic Sinica, 1998, 16(2): 154-161. (in Chinese)

[5] 杨爱玲, 郭荣伟. 埋入式进气道流场的雷诺应力测量和频谱分析[J]. 空气动力学报, 1999, 14(1): 80-86.
Yang A L, Guo R W. Measurement of the Reynold stresses and spectral analysis for the flow in a submerged air intake[J]. Acta Aerodynamic Sinica, 1999, 20(5): 450-454. (in Chinese)

[6] 任三星. 埋入式进气道设计与流场控制研究[D]. 南京航空航天大学, 1999.
Ren S X. Design and flow control investigation of a submerged air intake[D]. Nanjing University of Aeronautics and Astronautics, 1999. (in Chinese)

[7] 郭荣伟, 刘少永. 埋入式进气道设计[J]. 南京航空航天大学学报, 2002, 33(1): 8-12.
Guo R W, Liu S Y. Design of submerged inlet[J]. Journal of Nanjing University of Aeronautics and Astronautics, 2002, 33(1): 8-12. (in Chinese)

[8] 余安远, 郭荣伟. 一种隐身外形弹体下埋入式进气道的进气机理与低速实验研究[J]. 空气动力学报, 2003, 21(2): 182-188.
Yu A Y, Guo R W. Air-admission mechanism and low speed tunnel test of a submerged inlet with low RCS missile body[J]. Acta Aerodynamic Sinica, 2003, 21(2): 182-188. (in Chinese)

[9] 余安远, 郭荣伟. 隐身外形飞行器用埋入式进气道的设计及气动性能研究[D]. 南京航空航天大学, 2003.
Yu A Y, Guo R W. A study of the design and flow characteristics for a submerged inlet under a stealthy shaped fuselage[D]. Nanjing University of Aeronautics and Astronautics, 2003. (in Chinese)

[10] Taskinoglu Ezgi S, Knight D. Numerical analysis of submerged inlets[R]. AIAA 2002-3147, 2002.

[11] Taskinoglu Ezgi S, Knight D. Design optimization for submerged inlets-part I[R]. AIAA 2003-1247, 2003.

[12] Taskinoglu Ezgi S, Knight D. Design optimization for submerged inlets-part II[R]. AIAA 2003-3926, 2003.

[13] 孙姝, 郭荣伟. 平面埋入式进气道的口面参数选择与试验验证[J]. 航空学报, 2005, 26(3): 268-275.
Sun S, Guo R W. Experimental research of effects of entrance parameters on performance of submerged inlet[J]. Acta Aeronautica et Astronautica Sinica, 2005, 26(3): 268-275. (in Chinese)

[14] Tan H J, Guo R W. Design and wind tunnel study of a top-mounted diverterless inlet[J]. Chinese Journal of Aeronautics, 2004, 17(2): 72-78.

[15] 谭慧俊, 郭荣伟. 一种背负式无附面层隔道进气道的数值模拟与试验验证[J]. 航空学报, 2004, 25(6): 197-201.
Tan H J, Guo R W. Numerical investigation of a top-mounted diverterless inlet and its validation[J]. Acta Aeronautica et Astronautica Sinica, 2004, 25(6): 197-201. (in Chinese)

[16] 谭慧俊, 郭荣伟. 一种双斜切双压缩面进气道地面流态的数值模拟研究[J]. 航空学报, 2002, 23(3): 540-545.
Tan H J, Guo R W. Numerical simulation of a dual-swept/dual-ramp inlet under ground running[J]. Acta Aeronautica et Astronautica Sinica, 2002, 23(3): 540-545. (in Chinese)

Biographies:

SUN Shu Born in 1979, she is a graduate student in Nanjing University of Aeronautical and Astronautics at present. Her research interests focus on CFD and experimental investigation of internal flow. Tel: 025-84892206-2415, Email: susansun79@163.net